

The role of horizontal resolution for polar low simulations

Harold McInnes,^{a*} Jørn Kristiansen,^b Jón Egill Kristjánsson^a and Harald Schyberg^b

^a*Department of Geosciences, University of Oslo, Norway*

^b*Norwegian Meteorological Institute, Oslo, Norway*

*Correspondence to: H. McInnes, Department of Geosciences, University of Oslo, Forskningsparken Hus 8, Gaustadalleen 21, Oslo 0349, Norway. E-mail: h.m.innes@geo.uio.no

Polar lows are intense mesoscale cyclones that mainly occur during the winter over the sea in polar regions. Owing to their small spatial scale with a diameter between 200 and 1000 km, simulating polar lows is a challenging task. In this study we investigated how increased resolution of a numerical weather prediction model impacts its ability to simulate polar lows. We focused on a polar low that was successfully captured by three different flights during the IPY-THORPEX field campaign in 2008. Verifying model results against campaign data showed that decreasing the horizontal grid spacing from 12 to 4 km significantly improved the simulation of the developing polar low, and a further decrease to 1 km gave further improvement. A model run with latent heating reduced to 10% indicated an extensive influence of diabatic heating in this polar low case, and we suggest that the improved model performance at higher resolution could be connected to the model's handling of convection. Additional simulations starting 24 h later showed that the initial conditions were important for the model performance, and when simulating another polar low case we found that the model failed to produce the polar low independent of the resolution. This shows that while higher resolution indeed may give improved predictions of polar lows, other factors like synoptic situation, lateral boundaries and the initial condition may also be important. Copyright © 2011 Royal Meteorological Society

Key Words: polar low; IPY-Thorpex; horizontal resolution; latent heat

Received 5 November 2010; Revised 15 April 2011; Accepted 20 April 2011; Published online in Wiley Online Library 5 July 2011

Citation: McInnes H, Kristiansen J, Kristjánsson JE, Schyberg H. 2011. The role of horizontal resolution for polar low simulations. *Q. J. R. Meteorol. Soc.* 137: 1674–1687. DOI:10.1002/qj.849

1. Introduction

Increasing availability and reduced cost of computational power are opening the possibilities for operational weather forecasting centers to run high-resolution numerical weather prediction (NWP) models on an operational basis. While limited area models (LAMs) have been run operationally at 10–12 km horizontal grid spacing for many years, forecasting centers are currently moving towards horizontal grid spacing in the range 1–4 km, thus allowing for the representation of previously unresolved processes. It is commonly believed that this will give improved prediction

of mesoscale weather systems like thunderstorms, tropical cyclones and polar lows. A major benefit of increased resolution could be a more realistic treatment of moist convection, which is a major feature in many mesoscale systems. However, numerical studies of convective weather by Lean *et al.* (2008) and Niemelä and Fortelius (2005) revealed challenges connected to moist convection when increasing the horizontal resolution.

Polar lows are severe mesoscale cyclones that occur frequently over the sea in polar regions during the winter (Blechschmidt, 2008; Bracegirdle and Gray, 2008). There have been controversies over the definition of polar lows

during the last decades, especially with respect to wind speed and horizontal scale. Rasmussen and Turner (2003) stated the following useful definition: 'A polar low is a small, but fairly intense maritime cyclone that forms poleward of the main baroclinic zone (the polar front or other baroclinic zone). The horizontal scale of the polar low is approximately between 200 and 1000 km and surface winds near or above gale force.' In general, polar lows form when very cold air originating over the Arctic ice flows over the relatively warm sea, giving rise to strong heat fluxes from the sea surface to the atmospheric boundary layer, resulting in deep convection and release of latent heat in the troposphere. The heating produces a positive anomaly of potential vorticity (PV) at low levels which contributes to the development of a warm core cyclone. Idealized numerical experiments (Yanase and Niino, 2007) have indicated that both diabatic heating due to convection and baroclinic instability have important roles in the development of polar lows. Yanase and Niino performed simulations on an initial vortex with diabatic heating and sea surface fluxes turned on and off and with different degrees of baroclinicity in the zonal flow. They found that both baroclinicity and diabatic heating alone would induce cyclogenesis, but in the simulations with only diabatic heating, cyclogenesis would not take place if the initial vortex was too weak. These findings are consistent with Emanuel and Rotuno (1989), who pointed out that an initial disturbance of sufficient amplitude was needed to trigger cyclogenesis by air-sea interaction. This shows that while convection due to heat fluxes from the sea into the atmospheric boundary layer can have a major role in the intensification of a polar low, an initial vortex or some kind of triggering mechanism is required. A weakness of the Yanase and Niino (2007) study is that forcing from upper-level PV anomalies was not considered. In a case study of four different situations with favorable conditions for polar low development, Grønås and Kvamstø (1995) found the interaction between upper-level PV anomalies and low-level instability to be essential for the development of polar lows. The important interactions between upper-level forcing and low-level moist processes were also described in a numerical study of polar low dynamics by Montgomery and Farrell (1992).

The rapid and often unpredicted development of polar lows and the extreme weather often associated with them has been a threat to property and life and through history caused several fatal accidents at sea (Kolstad, 2006). Improved forecasts of polar lows would therefore be of great benefit for the population in high-latitude coastal areas and have been a strong motivation for research on these systems. However, due to a sparse network of observations at these latitudes, the observational basis for studies of polar lows has been weak. As a part of the Norwegian IPY-Thorpex project (Kristjánsson *et al.*, 2011), a major aircraft-based field campaign addressing weather systems in the Norwegian and Barents seas took place in February and March 2008. The objective was to improve forecasts of severe weather in the Arctic, and the campaign was carried out in order to provide observational data for this research. During three different flights on 3 and 4 March more than 50 dropsondes were released and the research team succeeded in capturing the pre-conditioning, development and mature stages of a polar low. Later in the campaign, on 17 March, a mature polar low was captured by dropsondes before it made landfall on the Norwegian coast near the Trondheim Fjord. The

field campaign produced a large amount of observational material, consisting of dropsonde data, *in situ* observations from the aircraft and data from two LIDAR instruments carried on board the aircraft.

In this study we will address the following question: will the use of higher resolution in NWP models lead to more accurate simulations of polar lows? The observations provided by the IPY-Thorpex campaign, together with satellite images, will help us to answer this question. In the current study we mainly focused on the 3–4 March polar low event, but the 17 March polar low was also assessed.

Owing to the extensive convection often associated with polar lows and the important role that diabatic heating may have in their development, we expect that a change in the model's resolution will have an impact on the simulation of these cyclones. A similar study by Lean *et al.* (2008) addressed convective weather over England in the summer season. The Unified Model (UM) from the UK Met Office was run at 12, 4 and 1 km horizontal grid spacing, and the predicted precipitation was verified against radar data. It was found that running UM at 4 and 1 km grid spacing gave a more realistic structure of showers than at 12 km grid spacing, and statistical verification of precipitation against radar data indicated that the model's performance improved as the resolution was increased. However, problems connected to the model's handling of convection at high resolution were also detected, such as the UM producing too few but too large convective cells when run at 4 km horizontal grid spacing and too many small cells when run at 1 km grid spacing.

Niemala and Fortelius (2005) performed similar numerical experiments on a case of shallow convection over Finland in May 2001. They performed simulations with 11, 5.6 and 2.8 km grid spacing in addition to modifications of the convection scheme. Verification against radar data indicated that 5.6 km grid spacing together with a fully grid size dependent convection scheme produced the most realistic distribution of showers.

These two studies show that increased horizontal resolution will not necessarily lead to improved simulations of convective weather but it has the potential to do so. Although polar lows are normally associated with extensive convection, both the time of year and location over sea make the present study substantially different from the studies mentioned above. The data available from the IPY-Thorpex campaign offer a unique opportunity to verify NWP simulations of polar lows.

2. Synoptic overview

We will here give a brief description of the two polar lows of this study. The first polar low formed during the afternoon of 3 March 2008 at the intercept of two frontal zones over the Norwegian Sea, where extremely cold air from the north met less cold air from the east and warmer maritime air from the south. The analysis from 1800 UTC 3 March 2008 overlaid on the satellite image from 1737 UTC the same day (Figure 1) shows that the polar low had started to develop at the western edge of an old synoptic scale low located at approximately 72°N and 15°E. Twelve hours later, at 0600 UTC 4 March, the old synoptic low still had approximately the same position, but the polar low had continued to develop and moved southeastwards

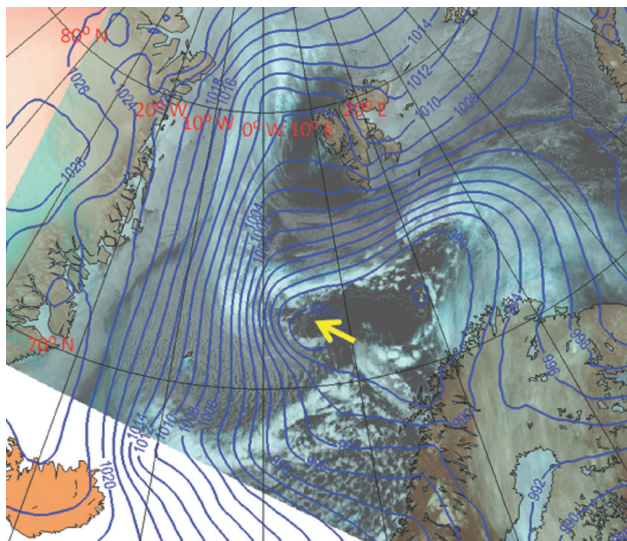


Figure 1. Sea-level pressure analysis from the Norwegian Meteorological Institute valid at 1800 UTC 3 March 2008 overlaid on a NOAA satellite image from 1737 UTC the same day. Yellow arrow indicates developing polar low.

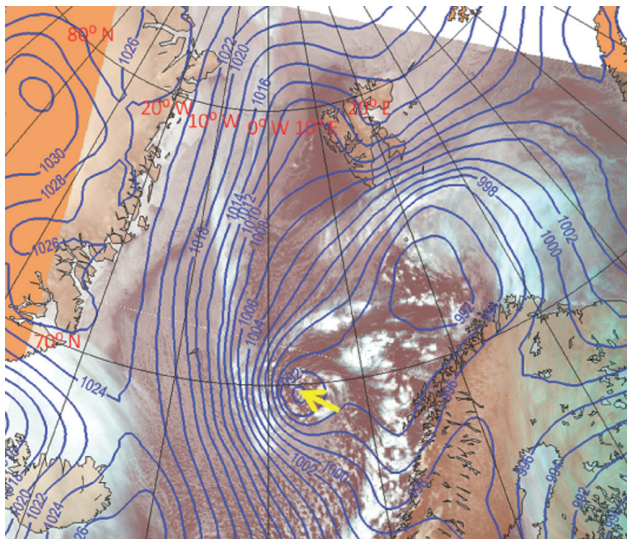


Figure 2. Sea-level pressure analysis from the Norwegian Meteorological Institute valid at 0600 UTC 4 March 2008 overlaid on a NOAA satellite image from 0547 UTC the same day. Yellow arrow indicates polar low.

to 70°N and 3°E (Figure 2). At 1200 UTC 4 March the polar low had reached 67°N and 4.5°E and started to decay (not shown), and it made landfall at the Norwegian coast at 65°N and 10°E during the evening. The reader is referred to Føre *et al.* (2011) for a more comprehensive description.

The second polar low investigated in this study occurred from 16 to 17 March and started to develop in a confluence zone with several vortices over the Norwegian Sea, shown in the satellite image from 0423 UTC 16 March (Figure 3). The NOAA image from 1236 UTC the same day (not shown) indicates that one of these vortices developed into a polar low that travelled southwestwards, and at 0050 UTC 17 March it was located at 68°N and 6°E and had developed a spiral-shaped cloud band (Figure 4). According to the satellite image from 0536 UTC (not shown) the polar low had continued to move towards the south and reached 66.5°N and 6.5°E. At this time it had started to fill, and

the decaying low reached the Norwegian coast a few hours later.

3. Numerical experiments

3.1. The model

We have used UM, which has been developed by the UK Met Office and is currently used by several forecasting centers around the world, e.g. the Norwegian Meteorological Institute, where the UM is run at 4 km horizontal grid spacing on a domain covering most of Scandinavia and adjacent seas. The dynamical core of the current version of the model is described by Davies *et al.* (2005) and includes a non-hydrostatic representation of the atmosphere, which is necessary at high resolution. It uses a terrain following vertical coordinate where the model surfaces gradually become horizontal at upper levels. Charney–Phillips staggering is applied in the vertical, while Arakawa C staggering is used horizontally. The horizontal grid is in latitude and longitude, and it is possible to rotate the grid in order to get quasi-uniform horizontal grid spacing within the domain when running the model on a limited area.

The UM has a mass flux convection scheme that is based on a single cloud model which represents an ensemble of clouds (Gregory and Rowntree, 1990). The cloud model applies parcel theory with entrainment and detrainment to represent the average characteristics of the entire cloud ensemble such as temperature, mass flux and humidity. The cloud model requires that cloud water content must exceed a minimum value and that the cloud must have reached a critical depth in order to give precipitation. The scheme has convectively available potential energy (CAPE) closure, where the mass flux initially depends on the stability of the lowest convective layer.

3.2. Experimental configuration

The main focus of this study was on the impact of altering horizontal grid spacing, and hence we ran the UM at 12, 4 and 1 km horizontal grid spacing. These are the main configurations of the UM in the present study and will hereafter be referred to as UM12, UM4 and UM1, respectively. In the vertical we used 70 levels for UM4 and UM1 and 38 levels were used for UM12, while the model lid was at 40 km for all configurations. When running the model, the time step was set to 300 s for UM12, 100 s for UM4 and 30 s for UM1. Except for the grid spacing and time steps, the main difference between these configurations is the treatment of convection. For UM1 the parameterization scheme for convection is turned off, allowing the model to treat all convection explicitly. A horizontal grid spacing of 1 km is considered to sufficiently resolve most of the convection, but this may not be the case at 4 km, where the grid spacing could be too large relative to the size of the convective clouds. Explicit treatment of convection would then tend to give too few showers that are too heavy (Lean *et al.*, 2008). However, if the convection is resolved at 4 km grid spacing, the use of the convection scheme may be problematic as it could lead to strong underestimation of precipitation (Lean *et al.*, 2008). A modified version of the convection scheme (Roberts, 2003) is therefore employed when running UM4. The CAPE Closure Timescale (CCT) is

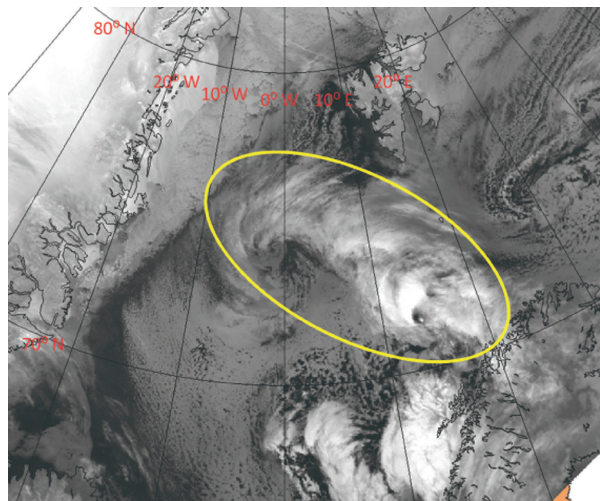


Figure 3. NOAA satellite image from 0423 UTC 16 March 2008. The yellow oval indicates the confluence zone with developing vortices.

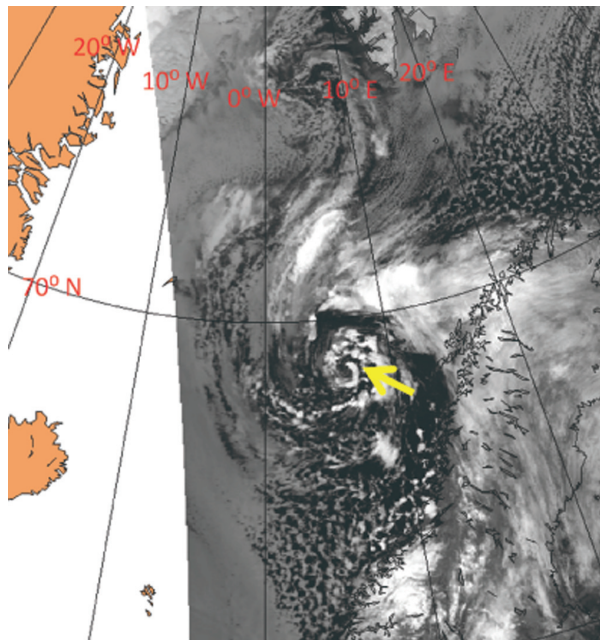


Figure 4. NOAA satellite image from 0050 UTC 17 March 2008. Yellow arrow indicates the polar low.

made dependent on the amount of CAPE so that CCT is longer when CAPE is large. A long CCT limits the activity of the convection scheme and allows the model to handle the convection explicitly. The assumption is that the size of convective clouds is dependent on the amount of CAPE, and hence large clouds would be handled explicitly. When running UM12 the resolution is too coarse to treat convection explicitly, and we therefore let all convection be represented by the convection scheme. However, the scheme was originally designed for larger grid spacing than 12 km and is based on the assumption that there are many clouds within a grid box. While this assumption is clearly problematic for 4 km grid spacing, one could according to Lean *et al.* (2008) also question this for 12 km grid spacing.

To isolate the impact of reduced horizontal grid spacing, we also ran the UM with 12 km horizontal grid spacing and 70 levels. In this configuration, which will be referred to as UM12_70L, we used a time-step of 100 s. We also

carried out a simulation with the UM4 configuration, where the latent heats of condensation and fusion were reduced to 10% of their initial values, and we will hereafter refer to this experiment as UM4_LH10. The different model configurations are summarized in Table I.

In the study of the 3–4 March polar low we applied all the main configurations as well as UM12_70L and UM4_LH10, while for the 16–17 March polar low we only ran UM12 and UM4. Figure 5 shows the domains for UM12, UM4 and UM1; the same UM12 and UM4 domains were used on both polar low situations. For UM12_70L and UM4_LH10 we applied the UM12 and UM4 domains respectively. The grid has been rotated in order to keep the size of the grid boxes quasi uniform within the domain (Davies *et al.*, 2005), placing the North Pole of the grids at 22°N and 140°E. The UM12 and UM4 domains contain 144 × 185 and 390 × 490 grid points respectively and cover the Norwegian Sea as well as parts of the Barents Sea and the North Atlantic. The UM1 was run on a much smaller domain due to high computational expenses. We selected a domain of 710 × 590 grid points (Figure 5), where we could capture the formation and early development of the 3–4 March polar low.

The start time of the model simulations of the 3–4 March polar low was set to 0000 UTC 2 March in order to capture the entire pre-conditioning that led to the cyclogenesis, and the forecast length was 60 h ending at 1200 UTC 4 March when the polar low was at its mature stage. To investigate the sensitivity to initial conditions, UM12 and UM4 were also started at 0100 UTC (hereafter referred to as UM12_01 and UM4_01) and 0200 UTC (hereafter referred to as UM12_02 and UM4_02) the same day (Table I). We further performed 48 h simulations starting at 0000 UTC 3 March with UM12 (hereafter referred to as UM12_24) and UM4 (hereafter referred to as UM4_24). For calculations with 12 and 4 km horizontal grid spacing, initial and lateral boundary data were interpolated from the High-Resolution Limited Area Model (HIRLAM; Undén *et al.*, 2002), which is run operationally at the Norwegian Meteorological Institute (met.no). The lateral boundaries were updated every hour, consisted of up to +13 h HIRLAM forecasts initialized every 0000 and 1200 UTC and entered the UM through a relaxation zone containing the eight outermost grid points of the UM domain. Scalars were bi-cubically interpolated from HIRLAM onto the UM grid, while wind vectors were modified according to the rotational direction of the UM grid relative to the HIRLAM grid (Kristiansen *et al.*, 2011). The HIRLAM forecasts benefited from data obtained during the campaign, since these were sent to the Global Telecommunications System (GTS). The UM calculations on 1 km horizontal grid spacing (UM1) used lateral and boundary data from the UM4 calculation.

The simulations of the 16–17 March polar low started at 1200 UTC 15 March and were run for 48 h, ending at 1200 UTC 17 March. As in the study of the 3–4 March polar low, we also here applied initial and lateral boundary data from HIRLAM. However, initializations of HIRLAM were not available after 15 March, so we used a 48 h forecast at the lateral boundary.

3.3. Pseudo-satellite images

As a part of the verifications of the model simulations of the 3–4 March polar low, we will study pseudo-satellite images from UM together with infrared satellite images.

Table I. Summary of the configurations for the UM. If not given under Comment, initialization time is 0000 UTC 2 March. UM12 and UM4 are also initialized at 1200 UTC 15 March.

Configuration	Time step	Number of levels	Comment
UM12	300 s	38	Main configuration
UM4	100 s	70	Main configuration
UM1	30 s	70	Main configuration
UM12_70L	100 s	70	
UM4_LH10	100 s	70	10% latent heat
UM12_01	300 s	38	Initialized 0100 UTC 2 March
UM4_01	100 s	70	Initialized 0100 UTC 2 March
UM12_02	300 s	38	Initialized 0200 UTC 2 March
UM4_02	100 s	70	Initialized 0200 UTC 2 March
UM12_24	300 s	38	Initialized 0000 UTC 3 March
UM4_24	100 s	70	Initialized 0000 UTC 3 March

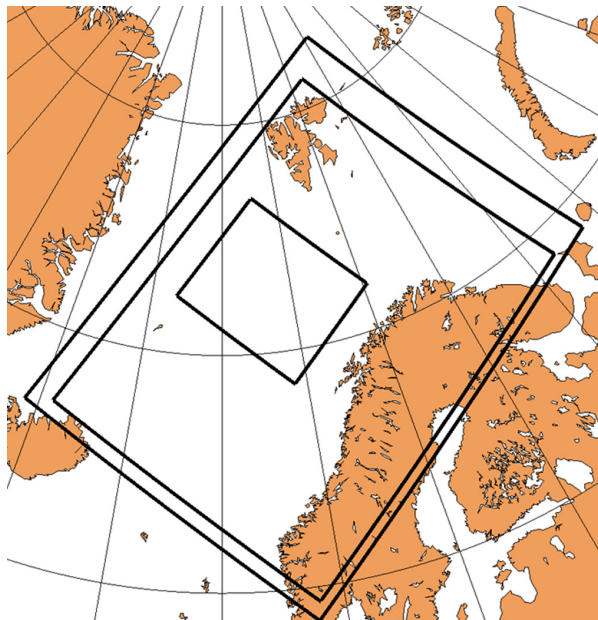


Figure 5. Domains for UM12 (outermost), UM4 (between) and UM1 (innermost). This figure is available in colour online at wileyonlinelibrary.com/journal/qj

The software for calculating the pseudo images, which was originally developed by Tijm (2004) and modified by Sørland (2009), estimates the cloud-top temperature. These pseudo images are in other words comparable to infrared satellite images. The routine runs through all model layers and if there is liquid or ice water present the cloud-top temperature is adjusted to the temperature at the current model level. If a cloud layer is more transparent than a pressure and temperature dependent threshold value, the adjustment of the cloud-top temperature is reduced.

4. Results and verification

4.1. 3–4 March 2008 case

We will start by assessing the 3–4 March polar low which formed during the afternoon of 3 March. Operational forecasts indicated that a polar low would form in the confluence zone at approximately 74°N, 5°E, and two different flights were carried out in order to capture the

pre-conditioning and formation of the polar low. During the first flight 20 dropsondes were launched between 1027 and 1328 UTC, while 15 dropsondes were launched between 1519 and 1742 UTC during the second flight. The track of these flights as well as the flight on 4 March are shown in Figure 6. We will here pay special attention to the formation of the polar low during the afternoon of 3 March and apply the dropsonde data from the flights to investigate the performance of the UM run at the different horizontal resolutions.

4.1.1. Simulations starting at 0000 UTC 2 March

An assessment of the sea level pressure (SLP) field over the first 24 h of the simulations (not shown) indicates that the different model configurations gave similar synoptic scale features in this period. After 12 more hours, at 1200 UTC 3 March, the SLP fields together with the 500–1000 hPa thickness (Figure 7) indicate that the predictions have started to diverge. The SLP field from UM12 (Figure 7(a)) indicates cyclogenesis at approximately 72°N and 10°E, while UM12_70L (Figure 7(b)) has a trough slightly further west at 8°E. The UM4_LH10 (Figure 7(c)) indicates cyclogenesis in the same area as UM12, while UM4 (Figure 7(d)) has a trough in the same area as UM12_70L. UM1 has produced a closed warm core low with a minimum SLP of 988 hPa at 72°N, 7.5°E (Figure 7(e)). We have assessed the SLP from the dropsondes released between 1027 and 1328 UTC, and found an SLP of 987 hPa in the same area that UM1 produced a closed low. This was the lowest SLP measured during the flight and indicates that UM1 as well as UM4 and UM12_70L have started to develop a cyclone at the approximately correct location.

We will now compare the predicted 925 hPa wind fields from the main configurations UM12, UM4 and UM1 valid at 1200 UTC (+36 h) with the wind data obtained from the dropsondes released between 1027 and 1328 UTC. We selected to verify the wind at this level in order to capture the low-level jet (Linders and Sætra, 2010), and at the same time avoid the influence of surface friction. Figure 8 shows the 925 hPa wind fields from UM12 (a), UM4 (b) and UM1 (c), together with measured wind at the same level. The wind from the dropsondes clearly shows an abrupt change in wind direction from northnorthwest to east, indicating a confluence zone at approximately 4°E, which is indicated by

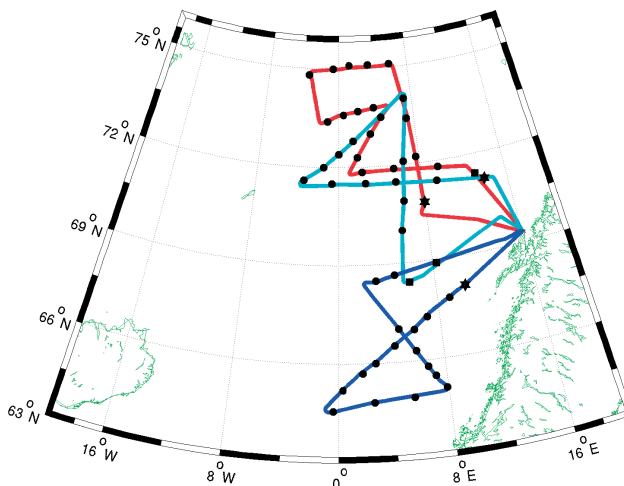


Figure 6. The flight tracks of the first flight (red) and second flight (light blue) on 3 March and the flight on 4 March (dark blue). The position of the first dropsonde in a flight is indicated by a hexagon, while a square indicates the last dropsonde. All other dropsonde positions are indicated by black dots.

a black curve in the figure. We further see that UM12 gives wind from the northnortheast, where the observations show northnorthwest and it also fails to predict wind direction in accordance with the observations east of the confluence line (Figure 8(a)), where it gives wind from the southeast that also is too strong compared to the observations. By contrast, UM4 and UM1 predict the wind direction very well, both of them reproducing the sudden change of wind direction from northnorthwest to east along the confluence line (Figure 8(b) and (c)), but they give too strong wind east of the line. Although the UM12 gives a change in wind direction in the same area, it is not as pronounced as the observations show, and we therefore see a strong indication of a better performance from UM4 and UM1. We also investigated the 925 hPa winds from the two additional UM configurations: UM12_70L and UM4_LH10 (not shown). The UM12_70L run gave a wind field almost identical to UM12 in most of the area, except for wind direction east of 72°N and 8°E. The wind field from UM4_LH10 has similarities to the wind field from UM4, but lacks the sudden change in wind direction associated with the confluence line. We further see that the model runs tend to underestimate the wind speeds measured to the west of the confluence line. At 75°N and 1°E the observation shows 25 m s⁻¹, while UM12 and UM4 give approximately 15 m s⁻¹ and UM1 gives 17 m s⁻¹. A comparison between SLP obtained from the dropsondes and data from the model runs indicates that the UM underestimates the horizontal pressure gradient in this area. Further southeast all model runs tend to overestimate the pressure gradient and hence the wind speeds.

Figure 9 shows the SLP field and the 500–1000 hPa thickness after 42 h of simulation, valid at 1800 UTC 3 March. The UM12 now has a closed 986 hPa cyclone at 71°N and 10°E (Figure 9(a)), which is too far east compared to what we see in the NOAA satellite image (Figure 1). The UM12_70L (Figure 9(b)) has a 988 hPa cyclone at 71°N and 7.5°E, while the SLP field from the UM4_LH10 run (Figure 9(c)) does not show any further cyclonic development compared to 6 h earlier. The UM4 (Figure 9(d)) has a 989 hPa closed cyclone at approximately the same location as UM12_70L, with a warm core that is still not completely secluded,

while UM1 (Figure 9(e)) now has a 987 hPa closed warm core cyclone located at 71°N and 6°E. The minimum SLP measured from the dropsondes deployed between 1519 and 1742 UTC was 984.8 hPa at 71.8°N and 6.3°E at 1709 UTC. UM12 does not simulate the location of the cyclone in accordance with the observations at this stage, while UM12_70L, UM4 and UM1 perform considerably better. The lack of cyclonic development in the UM4_LH10 run is a strong indication of diabatic heating being an important process in the development of this polar low, which is to be expected for a warm-core cyclone (Van Delden *et al.*, 2003).

We have compared the 925 hPa simulated wind field valid at 1800 UTC with the wind measured from the dropsondes deployed between 1519 and 1742 UTC, and have shown the measured and simulated wind from the main configurations UM12, UM4 and UM1 in Figure 10. When assessing wind direction we also see here that UM12 has problems. While the westernmost dropsondes show wind from the northwest, UM12 gives wind from the northnortheast in this area. Further southeast UM12 gives an easterly wind where the observations still show a northwesterly wind. The wind field from UM12_70L (not shown) is still very similar to the UM12 wind field, except in the area around 71°N and 7–10°E, where there is a difference due to the shift in position of the cyclone between these model runs (Figure 9(a) and (b)). In most cases UM4 and UM1 simulate wind direction very well. However, they fail at two locations near the center of the developing low, which is due to the developing low simulated by these model runs being located slightly further southsoutheast than the wind observations indicate. The wind field from UM4_LH10 (not shown) is similar to the wind field from UM4 in the northwestern part of the region shown in Figure 10(b), but they diverge strongly further southeast where UM4_LH10 lacks the developing cyclone. We may also here conclude that while UM fails to simulate the observed wind pattern accurately at 12 km horizontal grid spacing, a grid spacing of 4 or 1 km gives a realistic simulation. The highest wind speed measured was approximately 25 m s⁻¹ at 72°N and 0°E. At this position UM12 and UM4 give approximately 15 m s⁻¹, while UM1 gives 18 m s⁻¹. As was also noted 6 h earlier, UM underestimates the horizontal pressure gradient and hence the wind for the westernmost dropsondes, while there is some overestimation further east.

Both the confluence line and the evolving mesoscale cyclone are indicated by the wind fields from UM4 and UM1, and we may at this point conclude that UM4 and UM1 simulate the early development of the polar low realistically, while UM12 has problems. The improvement due to the decrease of horizontal grid spacing from 4 to 1 km is less pronounced, but UM1 seems to predict the highest wind speeds and the SLP of the developing cyclone slightly better than UM4. Although the large number of grid boxes within the UM1 domain indeed would allow the model to develop its own structure, the domain is slightly too small to capture the entire pre-conditioning area of the polar low. This could, together with the fact that the UM1 domain is nested within UM4, explain the relatively small difference between UM4 and UM1.

In order to shed more light over the differences between the simulations, we will assess the pseudo-satellite images from UM together with a conventional satellite image. Figure 11 shows the pseudo-satellite images from UM12 and UM4 valid at 1800 UTC 3 March, while the NOAA

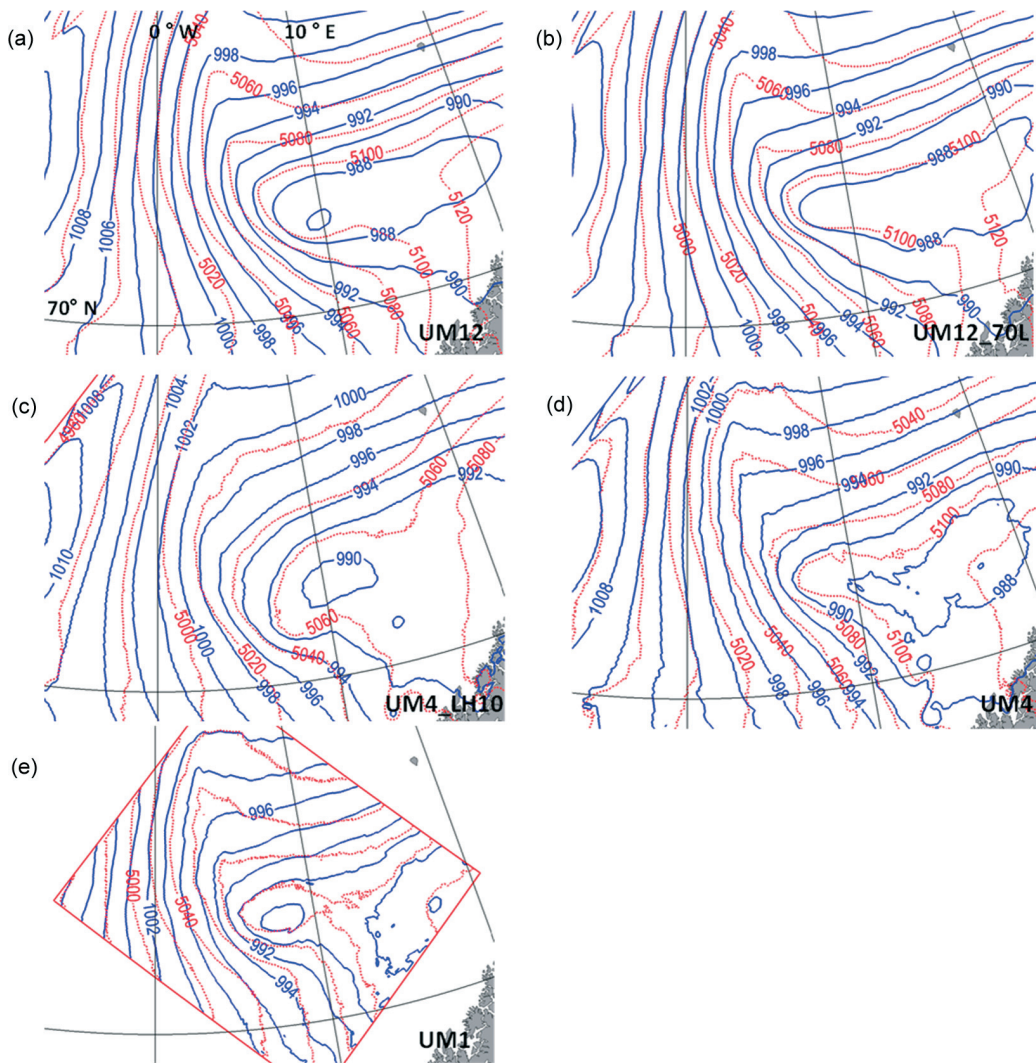


Figure 7. Sea-level pressure (blue, every 2 hPa) and 500–1000 hPa thickness (red, every 20 m) from 36 h simulations with UM12 (a), UM12_70L (b), UM4_LH10 (c), UM4 (d) and UM1 (e) valid at 1200 UTC 3 March.

image from 1737 UTC 3 March is shown in Figure 1. Both UM12 (Figure 11(a)) and UM4 (Figure 11(b)) reproduce the cloud band associated with the confluence zone fairly well, but UM12 places the intercept between the cloud bands approximately 5° too far east and slightly too far south. The UM4 also has a displacement of the intercept in the same direction, but less so than UM12. While the image from UM12 has continuous cloud bands, UM4 gives a structure of large convective cells that is more realistic compared to the satellite image. This could be a consequence of UM4 treating convection explicitly and hence producing convective cells, while convection is handled by the convection scheme in UM12. However, the pseudo image from UM4 has too few individual convective clouds compared to the NOAA image.

During the evening of 3 March and the night of 4 March the polar low continued its development as it travelled southwards, and at 0600 UTC 4 March the NOAA satellite image (Figure 2) indicates that it was positioned at 69.6°N and 3.1°E over the Norwegian Sea. The operational analysis from the Norwegian Meteorological Institute valid at 0600 UTC 4 March (Figure 2) indicates an SLP in the center of the low of approximately 990 hPa. The SLP fields and 500–1000 hPa thickness from UM valid at the same time (Figure 12) show that the UM12 (Figure 12 (a)) had

a 988 hPa cyclone at 68.7°N and 10.5°E , while UM12_70L (Figure 12 (b)) had placed the cyclone at approximately the same location as UM12. The run UM4_LH10 (Figure 12(c)) had at this stage developed a 994 hPa cyclone at 68.5°N and 12.7°E , which is approximately 400 km eastsoutheast of the polar low position indicated by the satellite image and close to the Lofoten Islands at the Norwegian coast. The UM4 (Figure 12(d)) had a 991 hPa cyclone at 68.1°N and 8.0°E , approximately 250 km too far southeast compared to the observed position. The 500–1000 hPa thickness field shows that while UM12, UM12_70L and UM4 gave a thickness of 5110–5130 m at the cyclone center, the UM4_LH10 run gave a considerably colder cyclone center with a thickness of approximately 5060 m, i.e. it does not develop a warm core in the centre of the polar low, which was found in the observations (Førre *et al.*, 2011).

We will now investigate the cyclone path from the operational analysis from met.no together with the path from the different model runs. Although the operational analyses will not give us the exact position of the polar low, an assessment of satellite images from 1200 to 1800 UTC 4 March UTC (not shown) indicates that the analyses positioned the cyclone fairly well. This is expected, since the analyses benefited from the observations obtained during the flights. In Figure 13 we show the positions of the cyclone at

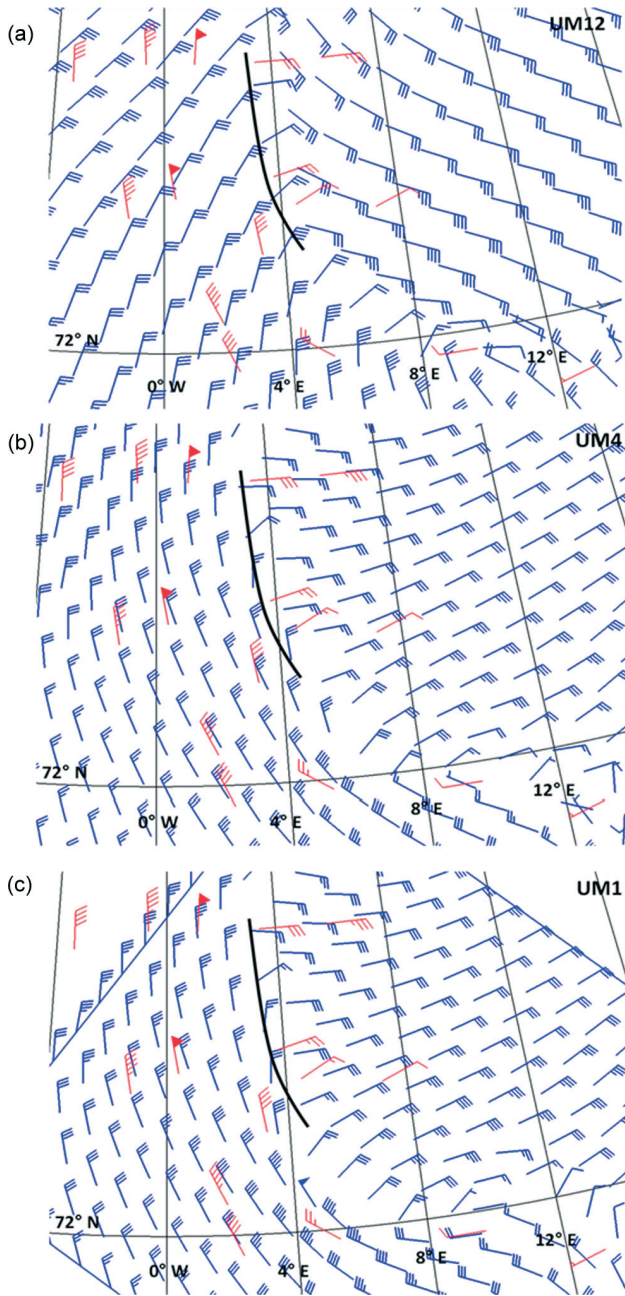


Figure 8. Wind measured from dropsondes (red) at 925 hPa and wind from 36 h simulations (blue) with UM12 (a), UM4 (b) and UM1 (c) valid at 1200 UTC 3 March 2008 at the same level. The blue wind bars represent the simulated wind in individual grid boxes and have been thinned to a legible density. The black curve indicates a confluence line based on observed wind.

6 h intervals for one day, starting at 1800 UTC 3 March. For 1800 UTC 4 March we only show the position in the analysis, since the model simulations ended at 1200 UTC 4 March. The polar low was not clearly shown in the analysis at 0000 UTC 4 March, and its position at that time is therefore not marked in the figure. The cyclone went out of the UM1 domain during the early hours of 4 March, and it is hence clear that UM4 gave the best path compared to the analyses when considering the whole period from 1800 UTC 3 March to 1200 UTC 4 March. However, UM4 displaced the cyclone towards the east between 1800 UTC 3 March and 0600 UTC 4 March, and it also moved it too quickly southwards. UM4 gave landfall at approximately 65°N, 10°E, in the same area as the analysis indicates landfall 6 h later. The other model

runs gave cyclone paths displaced towards the northeast, with UM4_LH10 being the worst, with landfall at 68°N, 15°E. At this stage we may conclude that decreasing the horizontal grid spacing from 12 to 4 km had a large positive impact on the simulations of both the formation and further development of the cyclone, even though the UM4 run had problems with respect to position.

4.1.2. Simulations starting at 0100 and 0200 UTC 2 March

While the model's performance for the current polar low case improved considerably due to increased resolution, NWP simulations are sensitive to the initial conditions and hence the start time of the model runs. In order to investigate the sensitivity to changes in the initial conditions, we carried out simulations with the UM12 and UM4 configurations starting at 0100 and 0200 2 March, which together with the simulations starting at 0000 UTC 2 March gave an ensemble with three time-lagged members. An assessment of the SLP fields from UM12_01 (not shown), UM12_02 (not shown) and UM12 (Figure 9(a)) indicates that there are only minor differences between these simulations at 1800 UTC 3 March. Also for UM4_01 (not shown), UM4_02 (not shown) and UM4 (Figure 9(d)) there were small differences in SLP distribution at 1800 UTC 3 March.

Figure 14(a) shows the SLP field from UM12, UM12_01 and UM12_02 valid at 0600 UTC 4 March, while Figure 14(b) shows the same for UM4, UM4_01 and UM4_02. At this time UM4_02 had displaced the polar low 80 km towards the northeast compared to UM4 (Figure 14(b)), while there still were only minor differences between the 12 km simulations. Despite the difference between the UM4 and UM4_02 at 0600 UTC 4 March, the assessment of the SLP fields indicates that all 4 km simulations performed better than the 12 km simulations.

4.1.3. Simulations starting at 0000 UTC 3 March

In order to further investigate the sensitivity to changes of initial conditions, simulations at 4 km and 12 km horizontal grid spacing were started at 0000 UTC 3 March. After 18 h, at 1800 UTC 3 March, the SLP fields from UM12_24 and UM4_24 were still quite similar and indicated cyclogenesis at 70°N, 10°E (not shown). By contrast, the operational analysis and the NOAA satellite image from 1737 UTC 3 March (Figure 1) indicated that the correct position was approximately 290 km northwest of this. During the next few hours the model runs started to diverge, and at 0600 UTC 4 March UM12_24 had created a trough at approximately 67°N, 10°E (Figure 15(a)) while UM4_24 had a 992 hPa cyclone 130 km further southwest (Figure 15(b)). This means that UM4_24 shifted the cyclone position approximately 200 km towards the south compared to the UM4 simulation starting 24 h earlier. However, 6 h later UM4_24 gave landfall of the cyclone at approximately 65°N, 11°E, which is the same area and time for landfall simulated by UM4. The UM12_24 had at this time positioned the cyclone in the same area as the UM12 simulation did. We have seen that when running at 4 km grid spacing, the ability of UM to simulate the formation and development of the cyclone was considerably reduced when starting 24 h later, in that the displacement between the simulated position and the position indicated by analysis and satellite image increased. With 12 km grid

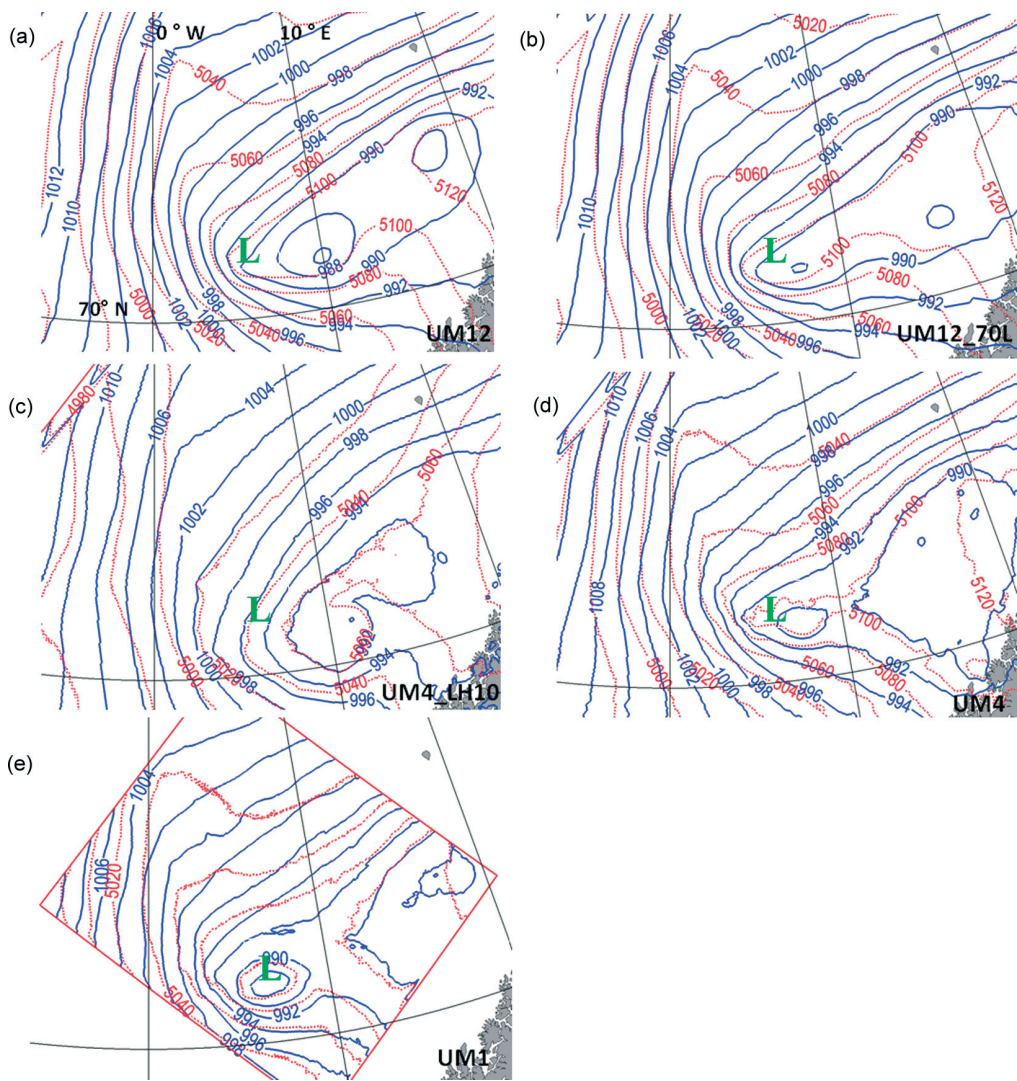


Figure 9. Sea-level pressure (blue, every 2 hPa) and 500–1000 hPa thickness (red, every 20 m) from 42 h simulations with UM12 (a), UM12-70L (b), UM4_LH10 (c), UM4 (d) and UM1 (e) valid at 1800 UTC 3 March. Green L is where dropsonde observations indicate developing cyclone.

spacing, UM performed poorly with start time 0000 UTC 3 March, as it did when it started 24 h earlier. The reduced performance of the 4 km simulations is consistent with the study of Kristiansen *et al.* (2011), where UM was used to run ensemble simulations of the same polar low. These simulations used 4 km horizontal grid spacing and the same domain as in the current study, but were started at 1800 UTC 2 March. The fact that the SLP distribution from the simulations of Kristiansen *et al.* at 1800 UTC 3 March was similar to the SLP distribution from UM4_24 (not shown) suggests that the reduced performance is not just a result of ensemble variability, but could be a consequence of starting the high-resolution simulation at a later stage and hence missing much of the pre-conditioning stage of the polar low.

4.2. 16–17 March case

We will here assess the UM12 and UM4 simulations of the polar low that developed during 16 March. Figure 16 shows the 24 h simulation of SLP and 500–1000 hPa thickness from UM12 (a) and UM4 (b) valid at 1200 UTC 16 March. While the NOAA image from 1236 UTC 16 March (not shown) indicates that a polar low had developed and was

positioned at 71.6°N and 10.5°E, both UM12 and UM4 had only a trough that was located approximately 300 km further northwest at 73.5°N, 3.5°E. Twelve hours later, the NOAA satellite image from 0050 UTC 17 March (Figure 4) shows that the polar low had moved approximately 380 km towards the southsouthwest and was located at 68.5°N and 6°E, while the 36 h runs from UM12 (Figure 17(a)) and UM4 (Figure 17(b)) valid at 0000 UTC 17 March had no sign of a cyclone in this area. Both simulations had moved the trough approximately 150 km towards the southeast. It was at this time located at 73°N, 8°E, and was less pronounced than 12 h earlier. In summary, we see that both the UM12 and UM4 run failed to capture the polar low, and it is therefore clear that increasing the resolution from 12 to 4 km did not influence the ability to simulate the polar low in this case. This contrasts sharply with the results from the 3–4 March case and will be discussed in the next section.

5. Summary and discussion

5.1. Summary

We have carried out numerical experiments with an NWP model on two different polar low cases in order to find

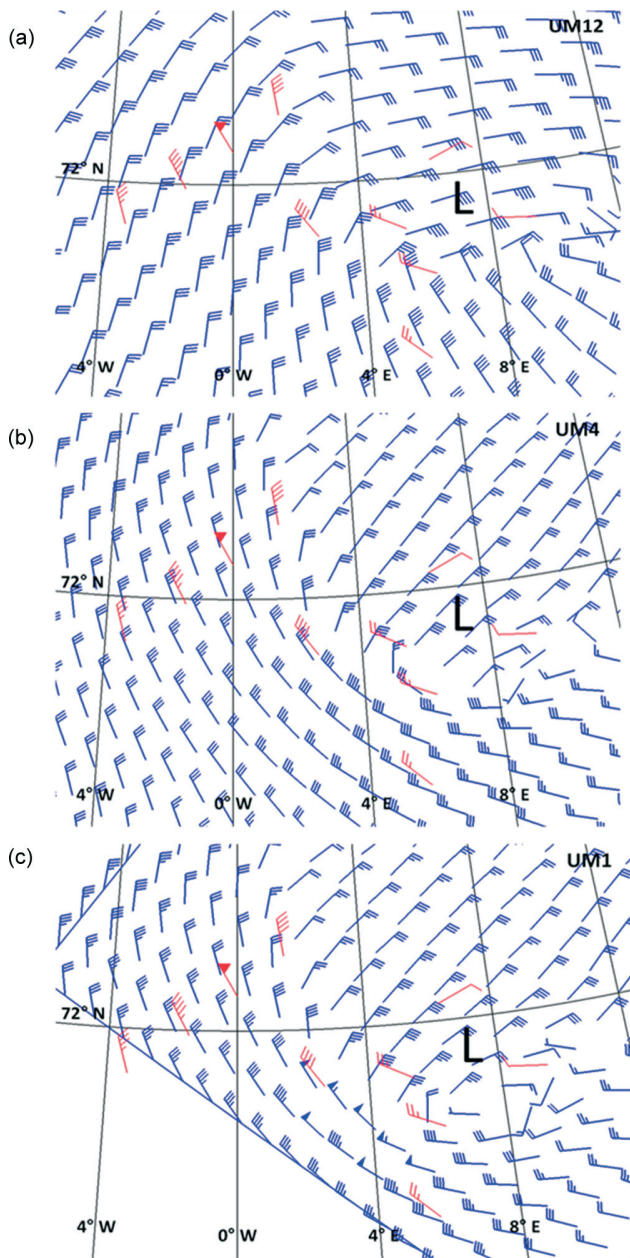


Figure 10. Wind measured from dropsondes (red) at 925 hPa and wind from 42 h simulations (blue) with UM12 (a), UM4 (b) and UM1(c) valid at 1800 UTC 3 March 2008 at the same level. The blue wind bars represent the simulated wind in individual grid boxes and have been thinned to a legible density. The black L is where observed wind indicates developing cyclone.

how increased resolution affects the model's ability to simulate polar lows. We used the UM from the UK Met Office and ran the model at 12, 4 and 1 km horizontal grid spacing. Our main focus was on a polar low that developed during the afternoon and evening of 3 March 2008 and was captured by dropsonde observations from three different flights. When verifying the different model runs against the observations, we have mainly focused on the formation and early development of the cyclone during 3 March. We started most of the simulations at 0000 UTC 2 March in order to give the model sufficient time to spin up and capture the entire pre-conditioning phase, while additional simulations were started 1, 2 and 24 h later.

The verification of the model simulations against dropsonde data from 3 March as well as assessment

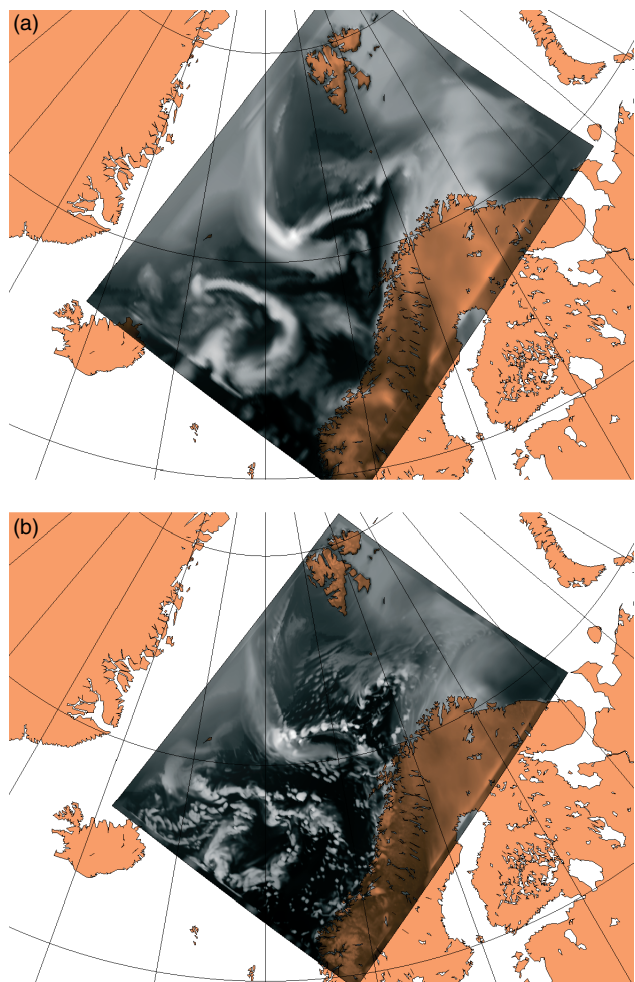


Figure 11. Pseudo-satellite images from 42 h simulations with UM12 (a) and UM4 (b) valid at 1800 UTC 3 March 2008.

of the pseudo-satellite images indicate that the model performed considerably better when horizontal grid spacing was reduced from 12 to 4 km. Wind measurements indicated a more realistic wind field from UM4 than from both UM12 and UM12_70L, and the pseudo images indicated that 4 km horizontal grid spacing gave a more realistic distribution of convection than 12 km. The observations of wind and SLP from the dropsondes indicate that a reduction of horizontal grid spacing from 4 to 1 km gave a further, but less pronounced improvement in performance. Both UM12_70L and UM12 gave cyclone paths that were displaced towards the northeast during the evening of 3 March and the early hours of 4 March, although the initial position of the cyclone from UM12_70L was better than from UM12. The UM4 gave a cyclone path that was more consistent with analyses and satellite images, although it placed the cyclone too far east during its early hours and moved it southwards too quickly. The reduction of latent heat to 10% both delayed and hampered the development of the polar low, and gave a cyclone path that was even more displaced towards the northeast than the model runs with 12 km horizontal grid spacing. While altering the start time from 0000 to 0100 or 0200 UTC 2 March turned out to have a relatively small impact on the simulations, starting the model 24 h later dramatically reduced the performance at 4 km grid spacing. When investigating the 16–17 March polar low we found that the difference between simulations

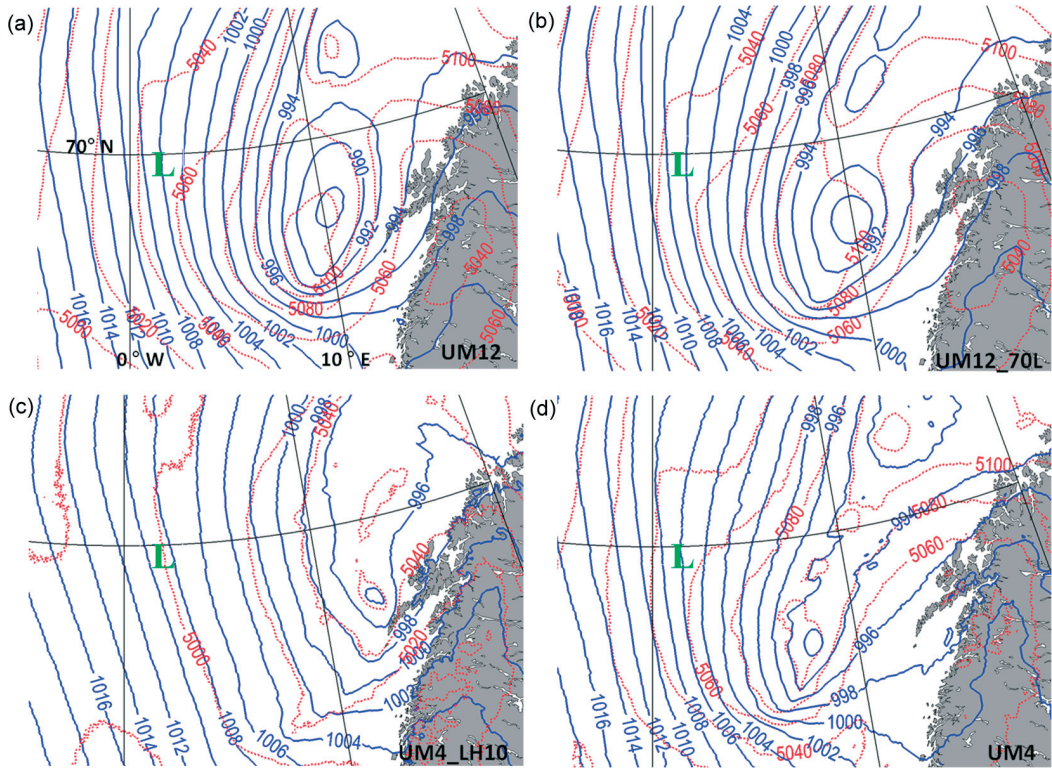


Figure 12. Sea-level pressure (blue, every 2 hPa) and 500–1000 hPa thickness (red, every 20 m) from 54 h simulations with UM12 (a), UM12_70L (b), UM4_LH10 (c) and UM4 (d) valid at 0600 UTC 4 March 2008. Green L shows cyclone position indicated by analysis.

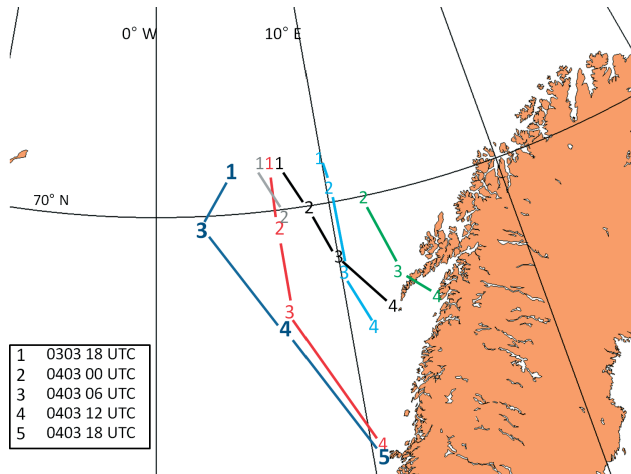


Figure 13. Position of polar low from UM12 (light blue), UM12_70L (black), UM4 (red), UM1 (gray), UM4_LH10 (green) and analysis (dark blue). For the analyses the position is shown between 1800 UTC 3 March and 1800 UTC 4 March at 6 h intervals, except for 0000 UTC 4 March. For the model runs the positions are shown between 1800 UTC 3 March and 1200 UTC 4 March with exceptions for UM4_LH10, where we have not shown the position for 1800 UTC 3 March and UM1, where we only have shown the positions for 1800 UTC 3 March and 0000 UTC 4 March.

at 12 and 4 km grid spacing was very small, and both failed to produce the polar low.

5.2. Discussion

When assessing the results one must keep in mind that different mechanisms such as low-level baroclinic instability, condensational heating due to convection, heating of the atmosphere from below as well as forcing from an upper-level PV anomaly may simultaneously contribute to the

development of a polar low. Linders and Sætra (2010) and Kristjánsson *et al.* (2011) investigated the observations of the 3–4 March polar low obtained from dropsondes and documented important features of the cyclone such as the frontal structure and the warm core. As well as revealing the strong baroclinicity associated with the confluence zone, they also found a slice of very dry air extending deep into the troposphere above the warm cyclone center. In an observational study of a mesoscale cyclone southeast of Greenland, McInnes *et al.* (2009) found by carrying out PV inversion that a similar dry slot was a strong indication of upper-level forcing. An analysis performed by Føre *et al.* (2011) indicates that both low-level baroclinic instability and upper-level forcing contributed to the development of the polar low. However, in order to explain why we get a better simulation of this cyclone when we run the model at 4 and 1 km grid spacing instead of 12 km, it would be useful to pay attention to convection and latent heating.

As described by Van Delden *et al.* (2003), latent heating at mid-tropospheric levels will create a positive PV anomaly at low levels and hence contribute to the deepening of a warm-core cyclone. It is therefore clear that the model's ability to handle convection is essential for a good simulation of the formation and deepening of a cyclone where latent heating has a significant role. The considerable difference between the simulations with original and reduced latent heating indicates this is an important mechanism in the 3–4 March case, and we will therefore address the handling of convection and precipitation in the different model configurations. The satellite image from 1737 UTC 3 March (Figure 1) and the pseudo images from 1800 UTC 3 March (Figure 11) indicate that UM4 was able to give a relatively realistic distribution of convective cells, while UM12 gave a widespread cloud band. The cloud band of UM12 may indicate

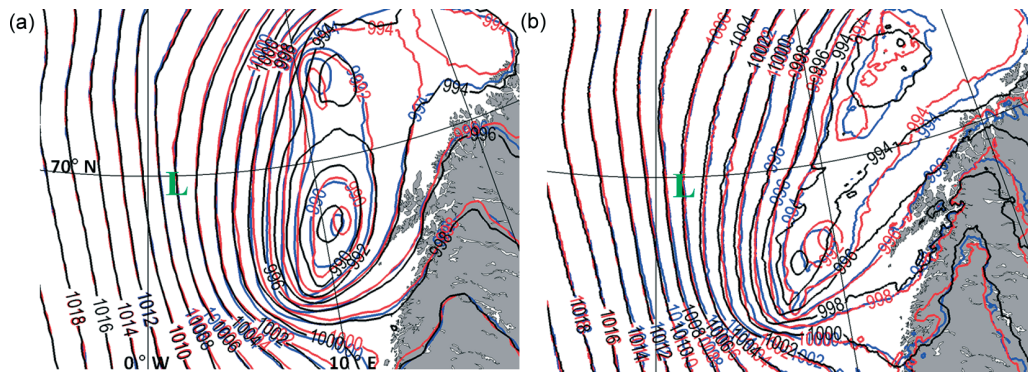


Figure 14. Sea-level pressure (every 2 hPa) from simulations initialized at 0000, 0100 and 0200 UTC 2 March valid 0600 UTC 4 March. (a) UM12 (black), UM12_01 (blue) and UM12_02 (red). (b) UM4 (black), UM4_01 (blue) and UM4_02 (red). Green L shows cyclone position indicated by analysis.

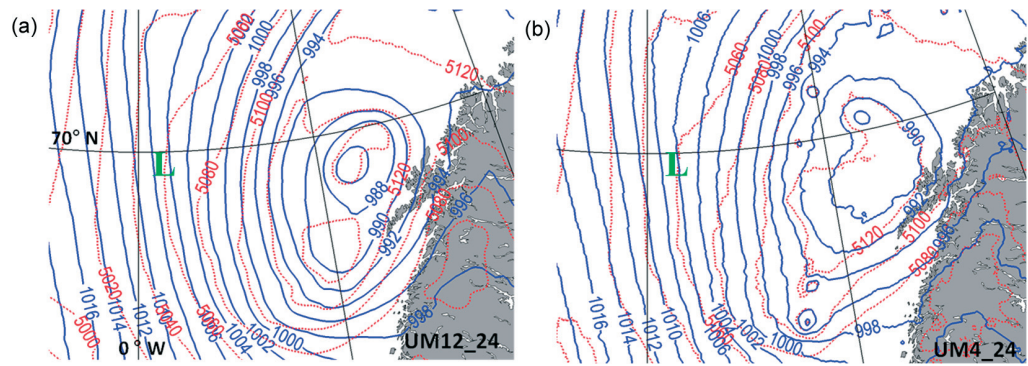


Figure 15. Sea-level pressure (blue, every 2 hPa) and 500–1000 hPa thickness (red, every 20 m) from 30 h simulations with UM12_24 (a) and UM4_24 (b) valid at 0600 UTC 4 March 2008. Green L shows cyclone position indicated by analysis.

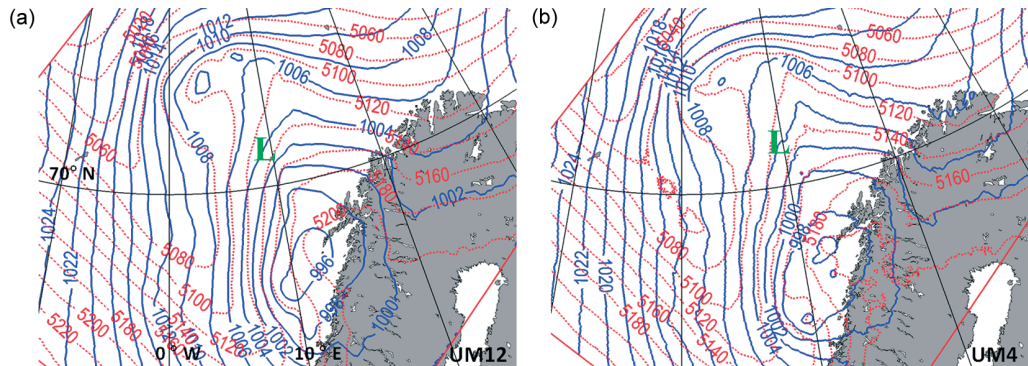


Figure 16. Sea-level pressure (blue, every 2 hPa) and 500–1000 hPa thickness (red, every 20 m) from 24 h simulations with UM12 (a) and UM4 (b) valid at 1200 UTC 16 March. Green L is where the satellite image indicates a polar low.

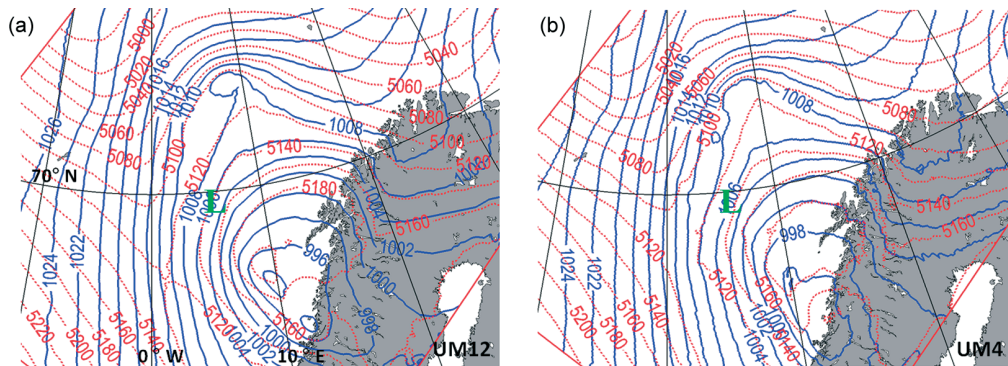


Figure 17. Sea-level pressure (blue, every 2 hPa) and 500–1000 hPa thickness (red, every 20 m) from 36 h simulations with UM12 (a) and UM4 (b) valid at 0000 UTC 17 March. Green L is where the satellite image indicates a polar low.

that the model produced too widespread condensational heating when run at 12 km horizontal grid spacing. The 1 h precipitation field from 1800 UTC 3 March (not shown) indicates a similar feature, with both UM1 and UM4 giving a horizontal distribution of precipitation with steep gradients and relatively high maximum values compared to the widespread and relatively weak precipitation from the simulations at 12 km grid spacing. In summary, we have seen that increasing the horizontal resolution of the model has a major impact on the distribution of convective clouds and precipitation. This indicates that the distribution of diabatic heating is strongly affected when the model's resolution is altered, and we would therefore argue that the improvement of the model performance experienced is connected to the handling of convective precipitation.

Our study has many similarities to the study of Lean *et al.* (2008), and a comparison would therefore be useful, although Lean *et al.* ran UM for considerably shorter periods than we did. One of the cases investigated by Lean *et al.* was a squall line over southeastern England, where the precipitation from the UM was compared to radar data. It turned out that UM was not able to reproduce the heavy precipitation associated with the squall line when run at 12 km horizontal grid spacing, while it produced heavy showers with a more realistic horizontal distribution when the grid spacing was reduced to 4 or 1 km. According to Lean *et al.*, 12 km grid spacing gave too widespread and light precipitation, while the heavy showers produced by UM on 4 or 1 km grid spacing were more consistent with the observations. The change in the structure of the precipitation field due to reduced grid spacing is indeed consistent with the findings in the present study (not shown).

For the 16–17 March case, both UM12 and UM4 failed to produce the polar low. The fact that UM4 failed to show any improvement compared to UM12 indicates that the problems in modeling this situation were not connected to the model's treatment of convection. Kristjánsson *et al.* (2011) pointed out that none of the operational models assessed during the Andøya field campaign were able to give a correct prediction of this polar low, and that this could possibly be explained by weak baroclinic forcing compared to the 3–4 March situation. When comparing the satellite image from 1737 UTC 3 March (Figure 1) and 0423 UTC 16 March (Figure 3), it is clear that the preconditioning stage of the 16–17 March case is more complicated, with several different vortices in a less distinct frontal zone than the one that occurred on 3 March. Another important difference in our modeling of this situation compared to the 3–4 March case is the use of 48 h predictions as boundary data. It is reasonable to believe that the quality of the lateral boundary data is not as good as in the 3–4 March situation, where we used forecasts that never exceeded 13 h and benefited from observations obtained during the flights on 3 March. In a study on the same case, Randriamampianina *et al.* (2011) carried out NWP simulations with analyses from ECMWF at the lateral boundary. These simulations also benefited from infrared atmospheric sounding interferometer (IASI) data and were able to simulate a polar low, although the position was too far west. This indicates that the poor model performance we experienced in this case can be partly attributed to the quality of the lateral boundary data. It is also reasonable to believe that the complexity of the situation with several different vortices contributed to our problems with the simulations.

6. Concluding remarks

Based on the present study of the two polar low cases, we may conclude that increasing the resolution of an NWP model may lead to considerable improvement in the simulation of a polar low. This is mainly due to a more realistic treatment of convection and condensational heating, and the potential of improvement is therefore highest in the cases where condensational heating has a significant role. The study showed that the impact of increasing horizontal resolution is case dependent. If the lateral boundary has low quality and the model fails to create the correct synoptic scale features, increasing the resolution will be of small value. The reduced performance of the 4 km simulations when starting them 24 h later was a surprising finding in this study. While we believe this could indicate that the 4 km simulations need to be initialized at a relatively early stage in order to create their own dynamics during the pre-conditioning of the polar low, we do not have sufficient evidence to argue strongly for this. The issue should be the subject of future research together with the sensitivity to the initial conditions. In conclusion, we would argue that the introduction of 4 km grid spacing in the Norwegian and Barents Seas has the potential to improve forecasts of polar lows on an operational basis. Additional improvement of the forecast by decreasing the grid spacing to 1 km would currently be difficult in practice, as this would require a domain that is much larger than the one used in the present study, and would hence be computationally very expensive. This should, however, be addressed in future studies, when sufficient computational power is available at a lower price.

Acknowledgements

This study has received support from the Norwegian Research Council through the project 'THORPEX-IPY: Improved forecasting of adverse weather in the Arctic – present and future' (grant no. 175992). We gratefully acknowledge Deutsches Zentrum für Luft- und Raumfahrt (DLR) for providing the dropsonde observations from their Falcon research aircraft. Dag Bjørge, Gunnar Noer, Bjørn Røsting, Trygve Aspelien, Øyvind Sætra, Viel Ødegaard and Silje Sørland from met.no gave technical and professional support during the study. We gratefully acknowledge Douglas Boyd and colleagues at the UK Met Office for support concerning the UM. The study received support from the Norwegian Research Council's Programme for Supercomputing through a grant of computing time. The simulations were carried out at the University in Trondheim (NTNU) and we acknowledge the HPC group at NTNU for technical support. We thank Gudmund Dalsbø, Ivan Føre and Camilla W. Stjern for practical support and useful discussions. We also acknowledge the two reviewers for valuable comments.

References

- Blechschmidt AM. 2008. A 2-year climatology of polar low events over the Nordic Seas from satellite remote sensing. *Geophys. Res. Lett.* **35**: L09815, DOI: 10.1029/2008GL033706.
- Bracegirdle TJ, Gray S. 2008. An objective climatology of the dynamical forcing of polar lows in the Nordic seas. *Int. J. Climatol.* **28**: 1903–1919.
- Davies T, Cullen MJP, Malcolm AJ, Mawson MH, Staniforth A, White AA, Wood N. 2005. A new dynamical core for the Met Office's global and regional modelling of the atmosphere. *Q. J. R. Meteorol. Soc.* **131**: 1759–1782.

- Emanuel KA, Rotunno R. 1989. Polar lows as arctic hurricanes. *Tellus* **41A**: 1–17.
- Føre I, Kristjánsson JE, Sætra Ø, Breivik Ø, Røsting B, Shapiro M. 2011. The full life cycle of a polar low over the Norwegian Sea observed by three research aircraft flights. *Q. J. R. Meteorol. Soc.* **137**: 1659–1673, DOI: 10.1002/qj.825.
- Gregory D, Rowntree PR. 1990. A mass flux convection scheme with representation of cloud ensemble characteristics and stability-dependent closure. *Mon. Weather Rev.* **118**: 1483–1506.
- Grønås S, Kvamstø NG. 1995. Numerical simulations of the synoptic conditions and development of arctic outbreak polar lows. *Tellus* **47A**: 797–814.
- Kolstad E. 2006. *Uvær*. J. W. Cappelens Forlag: Oslo.
- Kristiansen J, Sørland SL, Iversen T, Bjørge D, Køltzow MØ. 2011. High-resolution ensemble prediction of a polar low development. *Tellus* **63A**: 585–604.
- Kristjánsson JE, Barstad I, Aspelien T, Føre I, Hov Ø, Irvine E, Iversen T, Kolstad E, Nordeng TE, McInnes H, Randriamampianina R, Sætra Ø, Shapiro M, Spengler T, Olafsson H. 2011. The Norwegian IPY-THORPEX: polar lows and Arctic fronts during the 2008 Andøya campaign. *Bull. Am. Met. Soc.* (in press).
- Lean HW, Clark PA, Dixon M, Roberts NM, Fitch A, Forbes R, Halliwell C. 2008. Characteristics of high-resolution versions of the Met Office Unified Model for forecasting convection over the United Kingdom. *Mon. Weather Rev.* **136**: 3408–3424.
- Linders T, Sætra Ø. 2010. Can CAPE Maintain Polar Lows? *J. Atmos. Sci.* **67**: 2559–2571.
- McInnes H, Kristjánsson JE, Schyberg H, Røsting B. 2009. An assessment of a Greenland lee cyclone during the Greenland Flow Distortion experiment: an observational approach. *Q. J. R. Meteorol. Soc.* **135**: 1968–1985.
- Montgomery MT, Farrell BF. 1992. Polar low dynamics. *J. Atmos. Sci.* **49**(NO24): 2484–2505.
- Niemelä S, Fortelius C. 2005. Applicability of large-scale convection and condensation parameterization to meso-γ-scale HIRLAM: a case study of a convective event. *Mon. Weather Rev.* **133**: 2422–2435.
- Randriamampianina R, Iversen T, Storto A. 2011. Exploring the assimilation of IASI radiances in forecasting polar lows. *Q. J. R. Meteorol. Soc.* DOI: 10.1002/qj.838 (this issue).
- Rasmussen EA, Turner J. 2003. *Polar Lows Mesoscale Weather Systems in the Polar Region*. Cambridge University Press: Cambridge, UK.
- Roberts NM. 2003. The impact of a change to the use of the convection scheme to high-resolution simulations of convective events. *Met Office Technical Report*, 407.
- Sørland SL. 2009. *High-resolution ensemble forecasts of a polar low by non-hydrostatic downscaling*. Masters thesis in Geosciences, Meteorology and Oceanography, Department of Geosciences, University of Oslo.
- Tijm S. 2004. Hirlam pseudo satellite images. *Hirlam Newslet.* **46**: 59–64.
- Undén P, Rontu L, Järvinen H, Lynch P, Calvo J, Cats G, Cuxart J, Eerola K, Fortelius C, García-Moya JA, Jones C, Lenderlink G, McDonald A, McGrath R, Navascués B, Nielsen NW, Ødegaard V, Rodriguez E, Rummukainen M, Rööm R, Sattler K, Sass BH, Savijärvi H, Schreur BW, Sigg R, The H, Tijm A. 2002. *HIRLAM-5 Scientific Documentation, HIRLAM-5 Project*. SMHI: Norrkoping, Sweden.
- Van Delden A, Rasmussen EA, Turner J, Røsting B. 2003. Theoretical Investigations, in *Polar Lows Mesoscale Weather Systems in the Polar Region*, Rasmussen EA, Turner J. Cambridge University Press: Cambridge, UK; 286–404.
- Yanase W, Niino H. 2007. Dependence of polar low development on baroclinicity and physical processes: an idealized high-resolution numerical experiment. *J. Atmos. Sci.* **64**: 3044–3067.